

# HI 21cm absorption at $z \sim 3.39$ towards PKS 0201+113

N. Kanekar<sup>1</sup>★ J. N. Chengalur<sup>2,3</sup>, W. M. Lane<sup>4</sup>

<sup>1</sup>National Radio Astronomy Observatory, 1003 Lopezville Rd, Socorro, NM 87801, USA; <sup>2</sup>National Centre for Radio Astrophysics, Ganeshkhind, Pune-411007, India; <sup>3</sup>Australia Telescope National Facility, CSIRO, Epping, NSW 1710, Australia; <sup>4</sup>Naval Research Laboratory, Code 7213, 4555 Overlook Ave SW, Washington, DC 20375, USA

Received mmddyy/ accepted mmddyy

## ABSTRACT

We report the Giant Metrewave Radio Telescope detection of HI 21cm absorption from the  $z \sim 3.39$  damped Lyman- $\alpha$  absorber (DLA) towards PKS 0201+113, the highest redshift at which 21cm absorption has been detected in a DLA. The absorption is spread over  $\sim 115 \text{ km s}^{-1}$  and has two components, at  $z = 3.387144(17)$  and  $z = 3.386141(45)$ . The stronger component has a redshift and velocity width in agreement with the tentative detection of Briggs et al. (1997), but a significantly lower optical depth. The core size and DLA covering factor are estimated to be  $\lesssim 100 \text{ pc}$  and  $f \sim 0.69$ , respectively, from a VLBA 328 MHz image. If one makes the conventional assumption that the HI column densities towards the optical and radio cores are the same, this optical depth corresponds to a spin temperature of  $T_s \sim [(955 \pm 160) \times (f/0.69)] \text{ K}$ . However, this assumption may not be correct, given that no metal-line absorption is seen at the redshift of the stronger 21cm component, indicating that this component does not arise along the line of sight to the optical QSO, and that there is structure in the 21cm absorbing gas on scales smaller than the size of the radio core. We model the 21cm absorbing gas as having a two-phase structure with cold dense gas randomly distributed within a diffuse envelope of warm gas. For such a model, our radio data indicate that, even if the optical QSO lies along a line-of-sight with a fortuitously high ( $\sim 50\%$ ) cold gas fraction, the average cold gas fraction is low, ( $\lesssim 17\%$ ), when averaged over the spatial extent of the radio core. Finally, the large mismatch between peak 21cm and optical redshifts and the complexity of both profiles makes it unlikely that the  $z \sim 3.39$  DLA will be useful in tests of fundamental constant evolution.

**Key words:** galaxies: evolution: – galaxies: ISM – radio lines: galaxies

## 1 INTRODUCTION

While high redshift damped Lyman- $\alpha$  absorbers (DLAs), the highest HI column density systems seen in quasar spectra, are presumably the precursors of today’s galaxies and the primary gas reservoir for star formation, their size and structure have long been subjects of controversy (e.g. Wolfe et al. 2005). Understanding the nature of a “typical” DLA as a function of redshift is one of the important open problems in galaxy evolution.

HI 21cm absorption studies of DLAs towards radio-loud quasars provide an estimate of the harmonic mean spin temperature of the absorbing gas, via a comparison between the 21cm optical depth and the HI column density obtained from the Lyman- $\alpha$  line. This gives the distribution of gas in different temperature phases, which can be used to probe the redshift evolution of physical conditions in the absorbers (e.g. Kanekar & Briggs 2004). Further, a comparison between the redshifts of 21cm and optical metal-line

absorption (in a statistically large sample) can be used to study the evolution of a combination of fundamental constants (Wolfe et al. 1976). Extending 21cm absorption studies to the highest redshifts is interesting from both these perspectives. However, despite numerous searches, there are still only four confirmed detections of 21cm absorption in  $z > 1$  DLAs, out to  $z \sim 2.347$  (Wolfe & Davis 1979; Wolfe & Briggs 1981; Wolfe et al. 1985; Kanekar et al. 2006).

The  $z \sim 3.39$  absorber towards PKS 0201+113 (White et al. 1993) is one of the highest redshift DLAs known towards a radio-loud QSO and also has a very high HI column density ( $N_{\text{HI}} \sim 1.8 \times 10^{21} \text{ cm}^{-2}$ ; Ellison et al. 2001). Previous searches for 21cm absorption have yielded conflicting results, with two tentative detections (with substantially different redshifts, line depths and velocity spreads; de Bruyn et al. 1996; Briggs et al. 1997) and two non-detections at similar sensitivity (Briggs et al. 1997; Kanekar & Chengalur 1997), all using different radio telescopes. High resolution Keck spectroscopy found no metal lines at either of the putative 21cm redshifts, suggesting that the 21cm detections might have been spurious (Ellison et al. 2001). All the radio studies found evidence for a high spin temperature in the DLA, interpreted

\* E-mail: nkanekar@aoc.nrao.edu (NK); chengal@ncra.tifr.res.in (JNC); wendy.peters@nrl.navy.mil (WML)

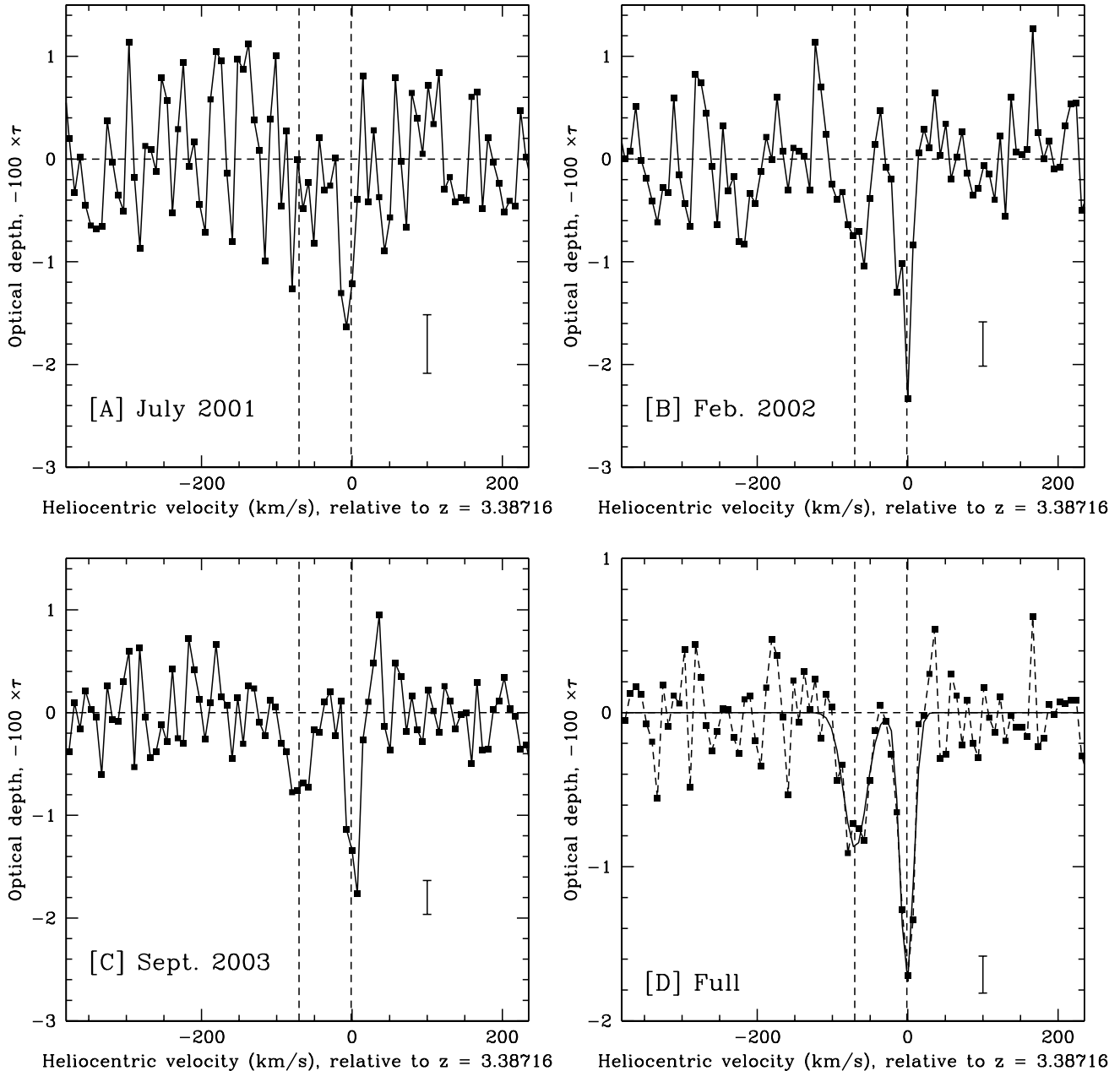


**Figure 1.** GMRT HI 21cm spectra towards PKS 0201+113 in [A] 2001 July, [B] 2002 February, and [C] September 2003, at the original velocity resolution of  $\sim 7.2 \text{ km s}^{-1}$ , with optical depth ( $-100 \times \tau$ ) plotted against heliocentric velocity, in  $\text{km s}^{-1}$ , relative to  $z = 3.38716$ . The main absorption component, close to zero velocity, is visible in all three spectra while the weaker component, at  $\sim -70 \text{ km s}^{-1}$ , can be seen in spectra [B] and [C], which have higher sensitivity. Panel [D] shows the final spectrum, after averaging the three spectra from [A]–[C]. The solid line in [D] shows the 2-Gaussian fit to the spectrum. The dashed vertical lines in each panel indicate the peaks of the two Gaussians of Table 1, while the error bar on the right side indicates the  $1\sigma$  noise on each spectrum.

as a large fraction of warm HI. In contrast, the strong CII\* lines in the Keck spectrum were used by Wolfe et al. (2003) to argue that the DLA contains a large fraction of cold HI. We report here on new deep Giant Metrewave Radio Telescope (GMRT) observations of the DLA in the redshifted HI 21cm line.

## 2 OBSERVATIONS AND DATA ANALYSIS

PKS 0201+113 was observed with the GMRT on multiple occasions, in 2001 January, 2001 July, 2002 February and 2003 September. The GMRT FX correlator was used as the backend in all runs, with a 1 MHz bandwidth divided into 128 channels centred at the expected redshifted 21cm line frequency, giving a velocity resolution of  $\sim 7.2 \text{ km s}^{-1}$ . The first three runs used the upper sideband of the correlator while the session in 2003 used the lower sideband. 19 antennas were available for the observations in 2001 January, 24

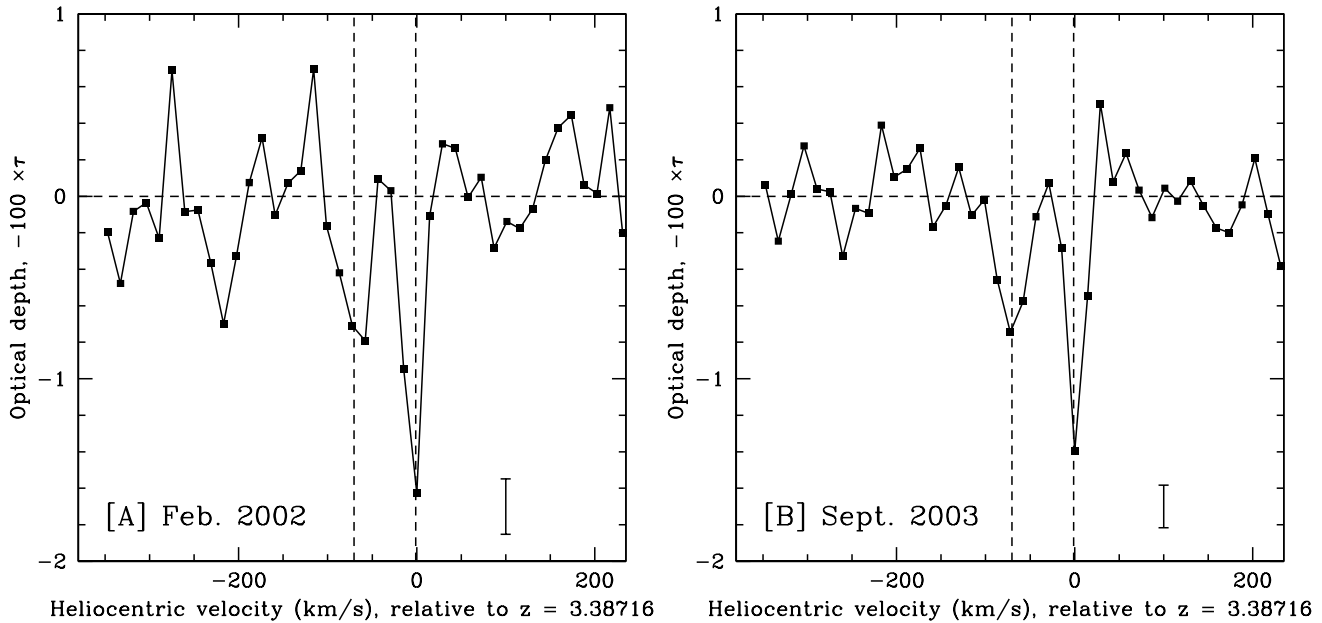


**Figure 2.** GMRT Hanning-smoothed and re-sampled HI 21cm spectra towards PKS 0201+113 from [A] 2002 February, and [B] September 2003, with optical depth ( $-100 \times \tau$ ) plotted against heliocentric velocity, in  $\text{km s}^{-1}$ , relative to  $z = 3.38716$ . The spectra have a velocity resolution of  $\sim 14.4 \text{ km s}^{-1}$ . The weaker component, at  $\sim -70 \text{ km s}^{-1}$ , is more clearly visible in both panels. The dashed vertical lines in each panel indicate the peaks of the two Gaussians of Table 1. The error bar on the right side of each panel indicates the  $1\sigma$  noise on the spectrum.

in July 2001, 28 in 2002 February and 27 in 2003 September. The varying UV-coverage is not a concern as PKS 0201+113 is unresolved by the longest GMRT baselines.

Observations of the standard calibrators 3C48 and 3C147 were used to calibrate the absolute flux density scale and the shape of the passband, while the compact source 0204+152 was used as the phase calibrator in all runs. The flux density of 0204+152 was measured to be within a few percent of 6 Jy, the 327-MHz value quoted in the Very Large Array (VLA) calibrator manual, in all cases except in 2001 July, when it was found to be  $5.62 \pm 0.04$  Jy. Note that the GMRT does not currently have online measurements of the system temperature; our experience indicates that the flux density scale is reliable to  $\sim 15\%$  in this observing mode.

Data from the different runs were converted to FITS and analysed separately in classic AIPS, using standard procedures. After initial editing and gain and bandpass calibration, around 50 channels (chosen to be away from the expected line location) were averaged together into a “channel-0” dataset and then used to obtain a continuum image of the field out to a radius of  $\sim 1$  degree, well beyond the half power of the GMRT primary beam. Data from different runs were imaged independently to test for source variability. The image was made by sub-dividing the field into 37 facets in all cases, to correct for the non-coplanarity of the array, and then used to self-calibrate the visibility data in an iterative manner until no further improvement in the image was obtained. This procedure typically converged after a few rounds of phase self-calibration, followed by two or three rounds of amplitude-and-phase self-calibration, with intermediate editing of corrupted data.

The task UVSUB was next used to subtract all continuum emission from the multi-channel U-V data and the residual visibilities inspected for any radio frequency interference (RFI) on all baselines, using the task SPFLG to view the time-frequency plane. All detected RFI was edited out. The continuum-subtracted U-V

data were shifted to the heliocentric frame (using the task CVEL) and imaged in all channels, and a spectrum then extracted from the image cube at the location of PKS 0201+113. Spectra were also extracted at the positions of other sources in the field to test for RFI. The data of 2001 January were found to be affected by low-level RFI and will hence not be discussed further; data from other epochs were found to be clean. The total on-source times were  $\sim 3$ , 7 and 10 hours in 2001 July, 2002 February and 2003 September, respectively, after all editing.

The 323 MHz flux density of PKS 0201+113 was measured to be 348 mJy, 417 mJy and 422 mJy in 2001 July, 2002 February and 2003 September, from the GMRT images. The typical RMS noise in these images, away from bright sources, is  $\sim 0.35 - 0.55 \text{ mJy/Bm}$ . While the flux density in 2001 July is  $\sim 17\%$  lower than in the other two runs, flux densities of other sources in the field (and the calibrator) were also lower by similar fractions; the GMRT data thus do not show any internal evidence for source variability. de Bruyn et al. (1996) obtained a flux density of  $(350 \pm 10)$  mJy with the Westerbork Synthesis Radio Telescope (WSRT) in 1991 February, marginally consistent with the GMRT values (given the  $\sim 15\%$  uncertainty in the GMRT flux scale); we were unable to compare flux densities of other sources in the 0201+113 field for the WSRT dataset. Briggs et al. (1997) measured  $(290 \pm 5)$  mJy in 1991 October with the VLA, significantly lower than the GMRT value. However, flux densities of other compact sources in the 0201+113 field in the VLA image are also lower (typically, by  $\sim 30\%$ ) than those in the GMRT image of 2003 September. Given the consistency of the GMRT and VLA measurements relative to field sources, we feel that the differences in measured flux density are unlikely to be caused by variability in 0201+113 itself. The GMRT flux density scale is likely to be correct, as the flux density of the calibrator, 0204+152, is in good agreement with that in the VLA calibrator manual. We will hence-

	$\tau_{\max}^*$ $\times 10^{-3}$	$\nu^{\dagger}$ MHz	$z$	FWHM <sup>‡</sup> (km s <sup>-1</sup> )
1	17.6(2.0)	323.7640(12)	3.387144(17)	$18.6 \pm 2.6$
2	8.8(1.5)	323.8400(34)	3.386141(45)	$35.1 \pm 7.4$

**Table 1.** Parameters of the 2-Gaussian fit to the final GMRT spectrum. Notes : \*Peak optical depth, using the GMRT flux density of 422 mJy. <sup>†</sup>Heliocentric frequency. <sup>‡</sup>Full width at half maximum.

forth use a flux density of 422 mJy (from 2003 September) as the GMRT measurement.

We also obtained a 328 MHz image of PKS 0201+113 with the Very Long Baseline Array (VLBA) in 2002, as part of a larger program to estimate the covering factors of quasars with foreground DLAs. The observations and data analysis will be described elsewhere; we merely note here that these data were analysed in the AIPS and DIFMAP packages, using standard procedures. The total on-source time was  $\sim 2$  hours.

### 3 SPECTRA AND RESULTS

The final spectra obtained in 2001 July, 2002 February and 2003 September are shown in panels [A]–[C] of Fig. 1, with optical depth (in units of  $-100 \times \tau$ ) plotted as a function of heliocentric velocity, relative to  $z = 3.38716$ . The spectra are at the original velocity resolution of  $\sim 7.2$  km s<sup>-1</sup> and have a root-mean-square (RMS) noise of 0.0057, 0.0043 and 0.0033 per channel, respectively, in units of optical depth (indicated by the error bars on the right side of each panel). The main absorption component, at  $\sim -1.0$  km s<sup>-1</sup>, can be clearly seen in all the spectra while a second, weaker, component is visible at  $\sim -70$  km s<sup>-1</sup> in the higher sensitivity spectra of panels [B] and [C]. The latter two spectra are shown in Figs. 2[A] and [B], after Hanning-smoothing and re-sampling to a velocity resolution of  $\sim 14.4$  km s<sup>-1</sup>, so that the weaker component can be seen more clearly. The doppler shift due to the Earth's motion between the three runs (e.g.  $\sim 42$  km s<sup>-1</sup> or  $\sim 45$  kHz between 2002 February and 2003 September) is far larger than the spectral resolution; both features are hence likely to be real.

Fig. 1[D] shows the final GMRT spectrum towards PKS 0201+113, obtained from a weighted average of the three optical depth spectra in panels [A]–[C] of Fig. 1. The RMS noise on this spectrum is 0.0024 per 7.8 kHz channel (in optical depth units) while the equivalent width of the absorption is  $\int \tau_{obs} dV = (0.714 \pm 0.017)$  km s<sup>-1</sup>. The solid line in Fig. 1[D] shows a two-Gaussian fit to the spectrum; the parameters of the fit are summarised in Table 1.

The 328 MHz VLBA image of PKS 0201+113, shown in Fig. 3, has an angular resolution of  $\sim 78 \times 38$  mas<sup>2</sup> (i.e.  $\sim 588 \times 290$  pc<sup>2</sup> at  $z \sim 3.39$ , the DLA redshift). The source is well-fit by a single elliptical Gaussian component; we measure a core flux density of  $\sim 292$  mJy and a deconvolved source size of  $17.6 \times 6.6$  mas<sup>2</sup> (i.e.  $\sim 132 \times 50$  pc<sup>2</sup> at  $z \sim 3.39$ <sup>1</sup>). A circular Gaussian model gives the same core flux density and an almost identical  $\chi^2$  for the fit; the deconvolved source size is then  $\sim 11.6 \times 11.6$  mas<sup>2</sup> (i.e.

<sup>1</sup> We use the standard  $\Lambda$ CDM cosmology throughout this paper, with  $\Omega_m = 0.27$ ,  $\Omega_\Lambda = 0.73$  and  $H_0 = 71$  km s<sup>-1</sup> Mpc<sup>-1</sup>

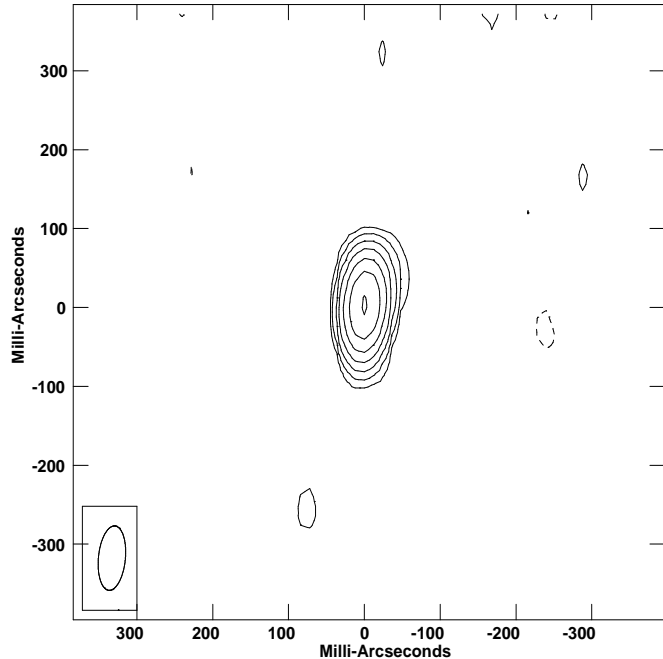


**Figure 3.** VLBA 328 MHz continuum image of PKS 0201+113, with a resolution of  $78 \times 38$  mas. The contours are at  $7.5 \times (-1, 1, 2, \dots, 64)$  mJy.

$\sim 87.5 \times 87.5$  pc at the absorber redshift). We note that attempts to fit an additional component to the marginal north-west extension did not significantly alter the core flux density.

### 4 DISCUSSION

In this section, results of the present GMRT observations are initially compared with earlier 21cm studies of the  $z \sim 3.39$  DLA. The gas kinematics of the DLA are briefly discussed before we compare the 21cm and optical low-ionization metal profiles, as a probe of fundamental constant evolution. We next derive the spin temperature of the absorbing gas under the standard assumption that the average HI column density towards the radio core is the same as that measured towards the optical QSO from the damped Lyman- $\alpha$  line. The comparison between metal line and 21cm profiles finds evidence for small-scale structure in the absorbing gas across the radio core, suggesting that the average column density against the radio core need not be the same as that towards the optical QSO. Finally, we discuss the HI temperature distribution in the light of the above results and two-phase models, and show that the gas must be predominantly warm in the absorber.

#### 4.1 A comparison with earlier 21cm absorption studies

As noted in the introduction, the  $z \sim 3.39$  DLA has been the focus of a number of 21cm absorption studies in the past, with very different results (de Bruyn et al. 1996; Briggs et al. 1997; Kanekar & Chengalur 1997). Details of the different observations are listed in Table 2, with the line depths quoted in both optical depth and flux density, while Fig. 4 shows a visual comparison between the GMRT spectrum and the earlier results. Note that the comparison in the figure is in flux density units (rather than in optical depth), as the continuum flux density estimates at Arecibo and the ORT are unreliable due to the very large beamwidths and the

Telescope	Epoch	Flux density mJy	Resolution $\text{km s}^{-1}$	RMS mJy	$\tau_{\max}^{\dagger} \times 10^{-2}$	Line depth <sup>†</sup> mJy	$z$	FWHM ( $\text{km s}^{-1}$ )	References
WSRT	1991	350	9.0	7.0	$8.5 \pm 2.0$	$30.0 \pm 7.0$	3.38699(3)	$9 \pm 2$	1
Arecibo	1993	318	4.5	4.1	$3.7 \pm 0.8$	$11.6 \pm 2.0$	3.38716(7)	$23 \pm 5$	2
VLA	1991	290	11.1	3.5	$1.5 \pm 1.2$	$4.2 \pm 3.4$	–	–	2
ORT	1997	–	5.6	3.7	$1.3 \pm 0.6$	$4.7 \pm 2.2$	–	–	3
GMRT	2001 – 2003	422	7.4	1.0	$1.76 \pm 0.20$ $0.88 \pm 0.15$	$7.43 \pm 0.84$ $3.71 \pm 0.63$	3.387144(17) 3.386141(45)	$18.6 \pm 2.6$ $35.1 \pm 7.4$	4

**Table 2.** A comparison between the 21cm spectra from different telescopes. <sup>†</sup>The quoted line and optical depths are from the Gaussian fits to the lines for the WSRT, Arecibo and GMRT spectra. For the VLA and ORT non-detections, the quoted line and optical depths are the values at 323.764 MHz (ORT) and 323.770 MHz (VLA), after smoothing the spectra to resolutions of  $\sim 16.8 \text{ km s}^{-1}$  (ORT) and  $\sim 22.2 \text{ km s}^{-1}$  (VLA), respectively, and resampling. The ORT optical depth uses the WSRT flux density of 350 mJy, as the ORT observation did not have a reliable simultaneous flux density measurement. Note that the WSRT and VLA values have *not* been scaled to the GMRT flux density value of 422 mJy but are on the original flux scales. References : (1) de Bruyn et al. (1996); (2) Briggs et al. (1997); (3) Kanekar & Chengalur (1997); (4) this paper.

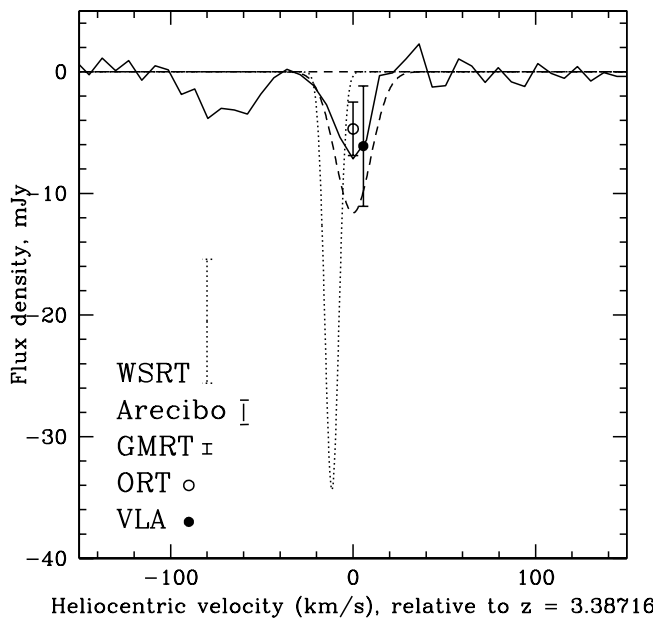


**Figure 4.** A comparison between the final GMRT spectrum (solid line) and earlier Arecibo, WSRT, VLA and ORT results, with flux density (in mJy) plotted against heliocentric velocity, in km/s, relative to  $z = 3.38716$ . The dashed and dotted lines show the Gaussian fits to the earlier tentative Arecibo and WSRT detections of Briggs et al. (1997) and de Bruyn et al. (1996), respectively. The solid and open circles (and  $1\sigma$  errors) indicate the values at 323.764 MHz (ORT) and 323.770 MHz (VLA) (Briggs et al. 1997; Kanekar & Chengalur 1997) respectively, after smoothing to resolutions of  $\sim 16.8 \text{ km s}^{-1}$  (ORT) and  $\sim 22.2 \text{ km s}^{-1}$  (VLA). The VLA and WSRT line depths have been scaled to the GMRT flux density of 422 mJy for the comparison. The  $1\sigma$  errors on the Arecibo, WSRT and GMRT fits are shown by the error bars to the right of each telescope name. See text for discussion.

associated confusion at the low observing frequency. The VLA and WSRT line depths have been scaled to the GMRT flux density of 422 mJy for the comparison.

It is clear from Fig. 4 and Table 2 that the VLA and ORT non-detections are consistent with the GMRT detection within the  $1\sigma$  errors; note that both spectra showed weak absorption (within the noise) close to the frequency of the main GMRT component ( $\sim 323.76 \text{ MHz}$ ). Next, the fit to the Arecibo feature of Briggs et al. (1997) is in excellent agreement with the stronger GMRT 21cm component in both redshift and FWHM. However, the peak optical depth is lower in the GMRT spectrum, discrepant at  $\sim 2.4\sigma$  level. Similarly, the Arecibo peak optical depth differs at  $\sim 2\sigma$  level from the ORT limit (Kanekar & Chengalur 1997) and is only in marginal agreement with the VLA non-detection (Briggs et al. 1997). A plausible cause of the optical depth discrepancy is an incorrect continuum flux density in the Arecibo data, a not-unusual problem with single-dish measurements. However, the line depth, in flux density units, in the Arecibo spectrum is also discrepant from the GMRT measurement at  $\sim 2\sigma$  level, implying that the difference in optical depths is not solely due to an error in the continuum flux density. As noted by Briggs et al. (1997), low-level RFI was present throughout the Arecibo spectrum (again, not uncommon for single-dish observations), resulting in non-Gaussian behaviour and possible systematic errors. This could well result in an incorrect determination of the Arecibo line depth and, hence, an over-estimate in the optical depth.

The only significantly discrepant result in Fig. 4 and Table 2 is the WSRT feature of de Bruyn et al. (1996), which is inconsistent with all the other data. The WSRT feature is unresolved and was detected at only  $\sim 4.5\sigma$  level in one polarization (de Bruyn et al. 1996); further these data have the lowest sensitivity of all the measurements. Given the difficulty of these low frequency observations in the presence of RFI, the relatively low statistical significance and the disagreement with all the other observations, the WSRT feature appears likely to be an artefact.

One possibility is that the above differences between the WSRT, Arecibo and GMRT features might be due to real changes in the optical depth of the 21cm absorption, as has been seen in two low  $z$  DLAs, towards AO 0235+164 (Wolfe et al. 1982)

and PKS 1127–145 (Kanekar & Chengalur 2001a). However, the GMRT spectra show no internal evidence for optical depth variability between the different observing epochs (from 2001 to 2003) and are also consistent with the VLA and ORT spectra (of 1991 and 1997), making optical depth variability an unlikely possibility. We hence conclude that (1) the WSRT feature of de Bruyn et al. (1996) is likely to be an artefact, (2) the GMRT, ORT, VLA and Arecibo spectra are consistent, if one assumes an incorrect estimate of the line depth in the Arecibo spectrum (note that the Arecibo spectrum is only discrepant at  $\sim 2\sigma$  level even without this assumption, with the FWHM and redshift in good agreement), and (3) there is no strong evidence for variability in the 21cm optical depth in the  $z \sim 3.39$  DLA. Of course, it is obvious from the RMS values of Table 2 that the second, weaker, feature seen in the GMRT spectrum is far too weak to have been detected in any of the earlier observations.

#### 4.2 Gas kinematics

The 21cm absorption profile of Fig. 1[D] has a total velocity spread (between nulls) of  $\sim 115 \text{ km s}^{-1}$ , the largest 21cm velocity width seen in any  $z \gtrsim 2$  DLA. In fact, this width is comparable to values seen in low  $z$  DLAs identified as bright spiral galaxies (for comparison, see Table 3 in Kanekar & Chengalur 2003). The only low  $z$  DLA with a 21cm velocity width larger than  $\sim 100 \text{ km s}^{-1}$  and *not* associated with a spiral disk galaxy is the  $z \sim 0.3127$  absorber towards PKS 1127–145 (Lane et al. 1998; Kanekar & Chengalur 2001a). Interestingly enough, Ellison et al. (2001) find the gas kinematics of the  $z \sim 3.39$  DLA towards PKS 0201+113 to be chaotic, with no evidence for an edge-leading asymmetry in the optical lines (a signature of a rotating disk; Prochaska & Wolfe 1997). Instead, the low-ionization metal lines show a large number of spectral components over a velocity spread of  $\sim 270 \text{ km s}^{-1}$ . Similarly, both 21cm components in the  $z \sim 3.39$  DLA are quite wide (see FWHMs in Table 1), perhaps due to multiple blended sub-components.

#### 4.3 Fundamental constant evolution

Comparisons between the redshifts of different spectral transitions can be used to probe evolution in the values of the fundamental constants such as the fine structure constant  $\alpha$ , the electron-proton mass ratio  $\mu \equiv m_e/m_p$ , the proton gyromagnetic ratio  $g_p$ , etc. A variety of approaches employing different transitions have been used, constraining changes in the above constants to be  $\lesssim 10^{-5}$  (e.g. Murphy et al. 2003; Srianand et al. 2004; Kanekar et al. 2005; Reinhold et al. 2006). One such technique uses optical metal lines and the 21cm line to probe changes in the quantity  $X \equiv g_p \mu \alpha^2$  (Wolfe et al. 1976). However, the velocity structure can be very different in the optical and radio lines, making it difficult to identify a single absorption redshift for the comparison, especially in cases where the profiles are complex, with multiple spectral components. While one might compare the redshifts of the strongest absorption component in the 21cm and metal lines (Tzanavaris et al. 2006), there is no physical reason why the strongest optical and 21cm absorption should arise in the same spectral component; this depends on local physical conditions in the absorbing clouds. The “strongest-component” approach thus introduces an extra source of systematic error that could lead to a bias in favour of a detection in small absorption samples. Conversely, while a comparison between the redshifts of “nearest-neighbour” absorption components in the 21cm and optical lines (Kanekar et al. 2006) might be viewed as a

test of the null hypothesis, it has the opposite bias, i.e. towards a non-detection of evolution.

The  $z \sim 3.39$  DLA towards PKS 0201+113 is the highest redshift absorber in which 21cm and optical lines have both been detected and is thus an obvious candidate for studies of changes in  $X \equiv g_p \mu \alpha^2$ . Unfortunately, both the 21cm and optical profiles are complex, extending over  $\gtrsim 100 \text{ km s}^{-1}$ , with multiple components. Fig. 5 shows the GMRT 21cm profile (histogram) overlaid on the unsaturated FeII- $\lambda 1122$  and CII\*- $\lambda 1335$  lines detected in the Keck-HIRES spectrum of Ellison et al. (2001). It can immediately be seen that even the strongest optical component is not uniquely determined; the absorption at  $\sim -65 \text{ km s}^{-1}$  is stronger in the FeII- $\lambda 1122$  transition while that at  $\sim -25 \text{ km s}^{-1}$  is stronger in the CII\* line. We will use the CII\* transition for the comparison, as this is expected to primarily arise in cold gas (Wolfe et al. 2003; hereafter W03), which also gives rise to the 21cm absorption. However, similar results are obtained on using other low-ionization metal species.

The CII\* absorption has three components, at  $z_A = 3.386821(7)$ ,  $z_B = 3.386297(10)$  and  $z_C = 3.386541(10)$ , in order of decreasing strength (the redshifts are indicated by the arrows in Fig. 5[B]), while the 21cm profile has two components, the main one at  $z_1 = 3.387144(17)$  and the secondary at  $z_2 = 3.386141(45)$ . A strongest-component comparison between the 21cm and CII\* lines (i.e. between  $z_A$  and  $z_1$ ) gives  $[\Delta X/X] = [\Delta z/(1 + \bar{z})] = (-7.4 \pm 0.4) \times 10^{-5}$ , where  $\Delta z = z_{\text{CII}*} - z_{21}$  and  $\bar{z} = (z_{21} + z_{\text{CII}*})/2$ . If this value of  $[\Delta X/X]$  is due to changes in  $[\Delta \alpha/\alpha]$  or  $[\Delta \mu/\mu]$ , it would require  $[\Delta \alpha/\alpha]$  or  $[\Delta \mu/\mu]$  to be nearly an order of magnitude larger than values obtained from other methods probing a similar redshift range<sup>2</sup> (Murphy et al. 2003; Srianand et al. 2004; Reinhold et al. 2006). Further, Tzanavaris et al. (2006) obtained  $[\Delta X/X] = (0.63 \pm 0.99) \times 10^{-5}$  over  $0.23 < z < 2.35$  from a strongest-component comparison between 21cm and optical lines in nine absorbers, again significantly smaller than the present value. This suggests that the difference between the redshifts of the strongest components towards PKS 0201+113 stems from intrinsic differences between the radio and optical sightlines, discussed further in the next section.

Alternatively, one might compare the redshifts of the weaker 21cm feature and its nearest-neighbour CII\* component (i.e. component B); formally, this yields  $[\Delta X/X] = (+3.6 \pm 1.0) \times 10^{-5}$ . However, these CII\* and 21cm components have very different velocity widths (FWHMs of  $\sim 13$  and  $\sim 21 \text{ km s}^{-1}$ , respectively), suggesting that at least part of the absorption does not arise in the same gas. A nearest-neighbour comparison between these optical and 21cm components is thus unlikely to yield reliable results. We hence conclude that, despite its high redshift, the  $z \sim 3.39$  DLA is unlikely to be useful for the purpose of probing fundamental constant evolution.

#### 4.4 Physical conditions in the absorber

The HI 21cm absorption in DLAs has generally been regarded as arising in a two-phase medium, with both cold (CNM) and warm (WNM) gas, similar to that seen in the Galaxy. Observational support for such a model has been found in the case of two low  $z$  DLAs (Lane et al. 2000; Kanekar et al. 2001). In the context of such two-phase models, the fact that high  $z$  DLAs generally have high spin temperatures (e.g. de Bruyn et al. 1996; Carilli et al.

<sup>2</sup> Note that changes in  $g_p$  are expected to be much smaller than those in  $\alpha$  and  $\mu$  (Calmet & Fritzsch 2002; Flambaum et al. 2004)

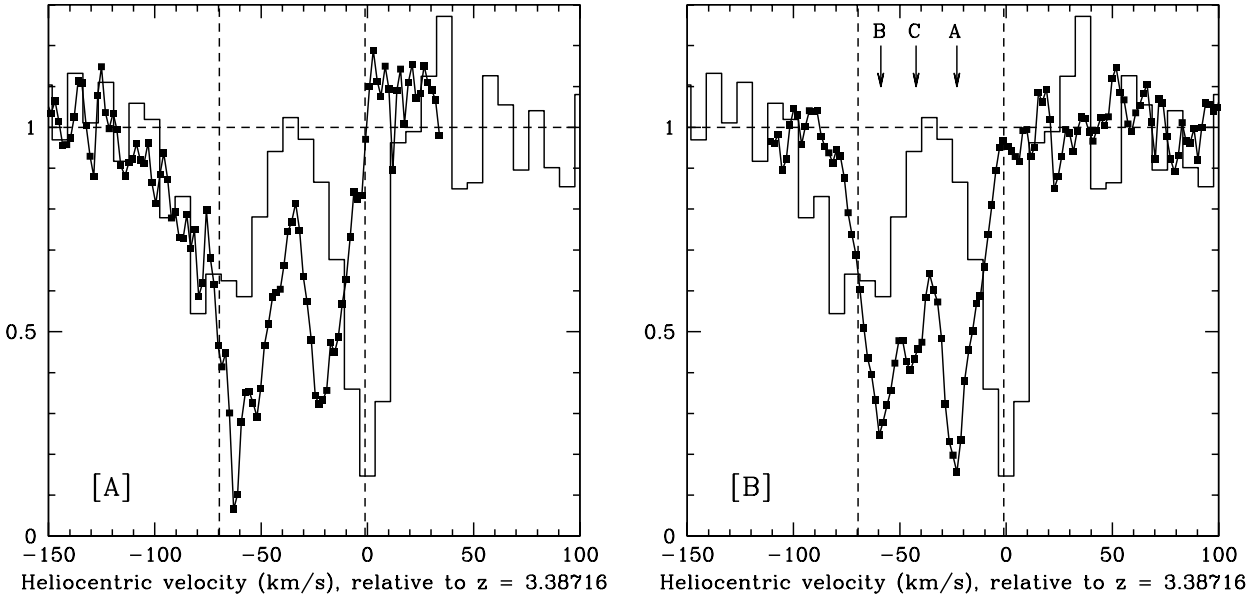


**Figure 5.** A comparison between the GMRT HI 21cm profile (histogram) and the [A] FeII  $\lambda 1122$  and [B] CII\*  $\lambda 1335$  Keck-Hires profiles (solid squares). The spectra are in arbitrary units and plotted against heliocentric velocity, in  $\text{km s}^{-1}$ , relative to  $z = 3.38716$ . The dashed vertical lines in each panel indicate the redshifts of the two 21cm components from the 2-Gaussian fit. The three vertical arrows in [B] indicate the redshifts of the three components (A, B and C) obtained from the fit to the CII\* line. See text for discussion.

1996; Kanekar & Chengalur 2001b, 2003) implies that the bulk of the gas is in the warm phase. Recently, however, W03 used the observed CII\* absorption in DLAs as a tracer of the cooling rate to argue that DLAs with strong CII\* lines must have a substantial fraction of their gas in the CNM phase [see, however, Srianand et al. (2005)]. W03 ruled out models in which all of the observed CII\* absorption arises in the WNM, finding that strong CII\* absorption requires that the line-of-sight includes some CNM [see also Wolfe et al. (2004)]. They further argued that the multiple lines of evidence suggesting that HI in high  $z$  DLAs consists primarily of warm gas (e.g. Liszt 2002; Norman & Spaans 1997; Kanekar & Chengalur 2003) are inconclusive, and suggested instead that a two-phase model with a CNM fraction of 50% towards the optical QSO is consistent with the observed bolometric luminosity in DLAs.

As noted by W03, the  $z \sim 3.39$  absorber towards PKS 0201+113 is one of only two high  $z$  DLAs that has both strong CII\* absorption (suggesting a high CNM fraction in the W03 model), as well as a high 21cm spin temperature. W03 resolved this apparent contradiction by arguing that the background radio core must subtend a linear diameter of  $\gtrsim 40$  pc at the DLA, while the CNM “clouds” in the absorber have linear sizes of  $\lesssim 10$  pc. They suggested that the strong CII\* absorption could be consistent with a lack of 21cm absorption if the CII\* absorption comes from a number of small CNM clouds lined up against the AU-sized optical QSO. We revisit this issue in the light of the new observations presented in the preceding sections.

A convenient starting point for this discussion is the general relation between 21cm optical depth  $\tau_{21}$ , total HI column density  $N_{\text{HI}}$  (in  $\text{cm}^{-2}$ ) along the path, and spin temperature  $T_s$  (in K) in the optically thin limit (Rohlfs & Wilson 2004),

$$N_{\text{HI}} = 1.823 \times 10^{18} T_s \int \tau_{21} dV , \quad (1)$$

where the integral is over velocity, in  $\text{km s}^{-1}$ . The spin temperature thus obtained is the column-density-weighted harmonic mean of the  $T_s$  values of different HI phases along the path. As such, it does not give the kinetic temperature of any individual phase but instead contains information on the distribution of gas in different temperature phases along the line of sight.

Next, the total flux density of the source measured by a short-baseline interferometer such as the GMRT or the VLA may be much larger than the flux density that is covered by the foreground absorbing “cloud” (e.g. Briggs & Wolfe 1983). This is especially true at the high redshift of the present observations; for example, the GMRT synthesized beam in the dataset of September 2003 is  $\sim 12.2'' \times 10.0''$ , subtending spatial dimensions of  $\sim 100 \times 75$  kpc at  $z \sim 3.39$ , far larger than the size of a typical galaxy. In such cases, the *measured* 21cm optical depth  $\tau_{\text{obs}}$  will be smaller than the “true” 21cm optical depth,  $\tau_{21}$ . If only a fraction  $f$  of the radio continuum is covered by the foreground absorbing gas, the “true” 21cm optical depth is given by  $\tau_{21} = (1/f) * \tau_{\text{obs}}$ . For a damped absorber, where the HI column density is measured from the Lyman- $\alpha$  line towards the optical QSO, we then have

$$N_{\text{HI}} = 1.823 \times 10^{18} (T_s/f) \int \tau_{\text{obs}} dV ; \quad (2)$$

$f$  is referred to as the 21cm covering factor of the DLA.

In addition to the assumption that the 21cm absorption is optically thin, Eqn. 2 contains two critical unknowns, the DLA covering factor  $f$ , and whether the HI properties along the line of sight to the optical QSO can be applied to the much larger line of sight towards the more-extended radio quasar core. The covering factor has been the subject of much discussion in the literature (e.g. Briggs & Wolfe 1983; Curran et al. 2005). In principle, the “true” 21cm optical depth can be directly determined by using VLBI techniques to map the 21cm absorption (e.g. Lane et al. 2000); however, this is usually impossible due to the fairly poor

frequency coverage and sensitivity of VLBI receivers. The alternative approach is to use VLBI observations at nearby frequencies to measure the fraction of flux density arising from the compact radio core. Even such measurements are rarely carried out in practice due to the technical difficulties in such VLBI studies at low frequencies (e.g. Briggs 1983). On the other hand, it is difficult, even in principle, to determine whether the HI distribution is uniform across the extended background radio source [see, for example, the discussions in de Bruyn et al. (1996) and W03]. Given that these two assumptions are generally untested in high  $z$  DLAs, the case of PKS0201+113 is doubly unusual in that we have meaningful VLBI constraints on the size of the radio core, and, as discussed below, also find observational evidence for small-scale structure in the HI 21cm absorbing gas.

For ease of comparison with earlier work, however, we first estimate the spin temperature of the  $z \sim 3.39$  DLA with the usual assumption that the HI gas is uniformly distributed across the radio core. If the 21cm absorber is a uniform slab covering the entire VLBI core, the covering factor  $f$  is  $S_{VLBA}/S_{GMRT} \sim (292/422) \sim 0.69$ . Further,  $N_{HI} = (1.8 \pm 0.3) \times 10^{21} \text{ cm}^{-2}$  (Ellison et al. 2001), and  $\int \tau_{obs} dV = (0.714 \pm 0.017) \text{ km s}^{-1}$ , which gives  $T_s \sim [(955 \pm 160) \times (f/0.69)] \text{ K}$ . This is in the “high” range of  $T_s$  values in DLAs (Kanekar & Chengalur 2003). We note that the above  $T_s$  value is significantly lower than the estimate  $T_s > 3290 \text{ K}$  in Kanekar & Chengalur (2003). This is because the latter assumed  $f \sim 1$  and a thermal velocity spread (FWHM = 20 km s $^{-1}$ ) which is much smaller than the true velocity spread of  $\sim 115 \text{ km s}^{-1}$ .

We next consider the assumption that the gas is uniformly distributed across the radio core. If the radio source were indeed very compact ( $\lesssim 10 \text{ pc}$ ), strong interstellar scintillation would be expected at the low GMRT observing frequencies, giving rise to a variable source flux density. However, the GMRT observations found no evidence for flux density variability over time-scales of a few years. It thus appears likely that the radio core is at least a few tens of parsecs in size at the redshifted 21cm frequency, far larger than the size of the optical core. Our VLBA observations cannot rule out this possibility as they only require the radio core to be smaller than  $\sim 100 \text{ pc}$ , the size of the fitted circular or elliptical Gaussian models.

The large difference in the sizes of the optical and radio cores implies that a comparison between the profiles of low ionization metal lines and the 21cm line would reveal the presence of small-scale velocity structure in the absorber over scales of tens of parsecs. This is because the low ionization metal lines trace the kinematics of the gas along the line of sight to the AU-sized optical QSO, while the 21cm line traces the kinematics along the much-larger ( $\gtrsim 40 \text{ pc}$ ) region lying in front of the radio core. No metal-line absorption can be seen in Figs. 5[A] and [B] at  $z \sim 3.387144$ , the redshift of the stronger 21cm component. As noted in Section 4.3, it is not possible to account for the large observed redshift difference between the 21cm and optical lines by fundamental constant evolution. Further, as pointed out by Ellison et al. (2001), the 21cm peak redshift is at the edge of the absorption seen in even the saturated OI- $\lambda 1302$  and CII- $\lambda 1334$  transitions (see Fig. 5 and the discussion in Ellison et al. 2001). This suggests that the stronger 21cm component does not arise along the line-of-sight to the optical core. While it is possible that the component arises against the extended radio emission that is resolved out in the VLBA image, this would require the absorbing clouds to be either very smooth and extended or, if compact, to have an extremely high 21cm optical depth. The more likely situation is that one or more compact CNM clouds cover part of the radio core, (but not the optical core)

and give rise to this 21cm component. In contrast, the weaker 21cm component lies close to the deepest FeII- $\lambda 1122$  and CII\* absorption and fairly strong metal-line absorption is seen over most of its velocity spread. This is consistent with at least part of the latter 21cm component arising from gas that does lie in front of the optical emission. The absorbing gas thus indeed appears to have structure on the scale of the radio core.

Despite the presence of this small-scale structure, it can be shown that if the HI is indeed in a two-phase medium as in the Galaxy, the WNM phase is likely to be dominant for the absorber as a whole, on the scales probed by the radio observations. This is because the HI in such two-phase models consists of randomly-distributed dense CNM “clouds” surrounded by a diffuse, widespread WNM envelope. If we assume that the optical QSO lies along a line of sight for which the CNM fraction is  $\sim 50\%$  (i.e. the scenario favoured by W03), the remaining half of the HI column density along this sightline is WNM, i.e.  $N_{WNM} \sim 9 \times 10^{20} \text{ cm}^{-2}$ . The number density in stable WNM is  $\lesssim 0.1 \text{ cm}^{-3}$  (Wolfire et al. 1995); a WNM cloud with  $N_{HI} \sim 9 \times 10^{20} \text{ cm}^{-2}$  must thus have a linear extent of  $\sim \text{few kpc}$  along the line-of-sight, far larger than the VLBA upper limit on the size of the radio core. The entire radio core must hence be covered by the WNM, with an average WNM column density of  $\sim 9 \times 10^{20} \text{ cm}^{-2}$ . Given the negligible 21cm optical depth of the WNM, the detected 21cm absorption components of Fig. 1[D] must arise in the CNM. Using a nominal CNM spin temperature of  $\sim 100 \text{ K}$ , the average CNM column density over the radio core (i.e. the core detected in the VLBA image) is  $N_{CNM} = 1.823 \times 10^{18} \times 100 \times (1/0.69) \times 0.714$ , i.e.  $N_{CNM} \sim 1.9 \times 10^{20} \text{ cm}^{-2}$ . The average CNM fraction across the radio core is hence  $N_{CNM}/(N_{CNM} + N_{WNM}) \sim 0.17$ . Thus, even if the line-of-sight to the optical QSO has a fortuitously high CNM fraction, the large-scale HI distribution must be dominated by the WNM.

We note that it is still possible to have a large fraction of the total HI in the CNM phase if the CNM were to be distributed in small “clouds” with velocity separations larger than the individual velocity widths, so that the absorption from each cloud lies below the GMRT 21cm detection threshold. As always for absorption studies, such a model, in which most of the CNM is “hidden”, cannot be ruled out from the absorption data alone.

## 5 SUMMARY

In summary, we report the GMRT detection of 21cm absorption from the  $z \sim 3.39$  DLA towards PKS 0201+113, with the 21cm profile consisting of two separate components spread over  $\sim 115 \text{ km s}^{-1}$ . The stronger of these components is in excellent agreement in both redshift and FWHM with the feature tentatively detected by Briggs et al. (1997) with the Arecibo telescope. We suggest that the higher peak optical depth measured by the latter could be due to a combination of an incorrect flux density scale and low-level RFI in the single-dish spectrum, resulting in an overestimate of the line depth. We find no significant evidence for optical depth variability in the 21cm line.

We obtain a covering factor of  $\sim 0.69$  from a 328 MHz VLBA image and use this to estimate an average spin temperature of  $T_s \sim [(955 \pm 160) \times (f/0.69)] \text{ K}$ , assuming that the average column density across the radio core is the same as that measured from the Lyman- $\alpha$  line. A comparison between the optical low-ionization metal-line and 21cm profiles finds evidence for structure in the absorbing gas across the radio core, bringing the above assumption

into question. Despite this, the GMRT observations indicate that most of the HI towards the radio core must be in the warm phase, even if a high CNM fraction is present on the narrow sightline towards the optical QSO. Finally, the complexity of the 21cm and CII\* absorption lines and the large offset between peak optical and 21cm redshifts suggests that the  $z \sim 3.39$  DLA is unlikely to be of use in probing fundamental constant evolution.

## 6 ACKNOWLEDGMENTS

We thank Sara Ellison, Elias Brinks and Frank Briggs for respectively providing us with the Keck-Hires spectrum towards PKS 0201+113, a VLA 327 MHz image of the PKS 0201+113 field and a postscript version of the VLA 21cm spectrum, and Ayesha Begum for carrying out the GMRT observations of 2003 September. We also thank the staff of the GMRT who made these observations possible. The GMRT is run by the National Centre for Radio Astrophysics of the Tata Institute of Fundamental Research. Basic research in radio astronomy at the Naval Research Laboratory is supported by 6.1 base funding. The National Radio Astronomy Observatory is operated by Associated Universities, Inc, under co-operative agreement with the National Science Foundation.

## REFERENCES

Briggs F. H., 1983, AJ, 88, 239  
 Briggs F. H., Brinks E., Wolfe A. M., 1997, AJ, 113, 467  
 Briggs F. H., Wolfe A. M., 1983, ApJ, 268, 76  
 Calmet X., Fritzsch H., 2002, Eur. Phys. Jour. C, 24, 639  
 Carilli C. L., Lane W. M., de Bruyn A. G., Braun R., Miley G. K., 1996, AJ, 111, 1830  
 Curran S. J., Murphy M. T., Pihlström Y. M., Webb J. K., Purcell C. R., 2005, MNRAS, 356, 1509  
 de Bruyn A. G., O'Dea C. P., Baum S. A., 1996, A&A, 305, 450  
 Ellison S. L., Yan L., Hook I. M., Pettini M., Wall J. V., Shaver P., 2001, A&A, 379, 393  
 Flambaum V. V., Leinweber D. B., Thomas A. W., Young R. D., 2004, Phys. Rev. D, 69, 115006  
 Kanekar N., Briggs F. H., 2004, New Astr. Rev., 48, 1259  
 Kanekar N., Carilli C. L., Langston G. I., Rocha G., Combes F., Subrahmanyan R., Stocke J. T., Menten K. M., Briggs F. H., Wiklind T., 2005, Phys. Rev. Lett., 95, 261301  
 Kanekar N., Chengalur J. N., 1997, MNRAS, 292, 831  
 Kanekar N., Chengalur J. N., 2001a, MNRAS, 325, 631  
 Kanekar N., Chengalur J. N., 2001b, A&A, 369, 42  
 Kanekar N., Chengalur J. N., 2003, A&A, 399, 857  
 Kanekar N., Ghosh T., Chengalur J. N., 2001, A&A, 373, 394  
 Kanekar N., Subrahmanyan R., Ellison S. L., Lane W. M., Chengalur J. N., 2006, MNRAS, 370, L46  
 Lane W., Smette A., Briggs F., Rao S., Turnshek D., Meylan G., 1998, AJ, 116, 26  
 Lane W. M., Briggs F. H., Smette A., 2000, ApJ, 532, 146  
 Liszt H., 2002, A&A, 389, 393  
 Murphy M. T., Webb J. K., Flambaum V. V., 2003, MNRAS, 345, 609  
 Norman C. A., Spaans M., 1997, ApJ, 480, 145  
 Prochaska J. X., Wolfe A. M., 1997, ApJ, 487, 73  
 Reinhold E., Buning R., Hollenstein U., Ivanchik A., Petitjean P., Ubachs W., 2006, Phys. Rev. Lett., 96, 151101  
 Rohlfs K., Wilson T. L., 2004, Tools of Radio Astronomy. Berlin: Springer, 2004  
 Srianand R., Chand H., Petitjean P., Aracil B., 2004, Phys. Rev. Lett., 92, 121302  
 Srianand R., Petitjean P., Ledoux C., Ferland G., Shaw G., 2005, MNRAS, 362, 549  
 Tzanavaris P., Webb J. K., Murphy M. T., Flambaum V. V., Curran S. J., 2006, MNRAS, accepted (astro-ph/0610326)  
 White R. L., Kinney A. L., Becker R. H., 1993, ApJ, 407, 456  
 Wolfe A. M., Briggs F. H., 1981, ApJ, 248, 460  
 Wolfe A. M., Briggs F. H., Davis M. M., 1982, ApJ, 259, 495  
 Wolfe A. M., Briggs F. H., Turnshek D. A., Davis M. M., Smith H. E., Cohen R. D., 1985, ApJ, 294, L67  
 Wolfe A. M., Broderick J. J., Condon J. J., Johnston K. J., 1976, ApJ, 208, L47  
 Wolfe A. M., Davis M. M., 1979, AJ, 84, 699  
 Wolfe A. M., Gawiser E., Prochaska J. X., 2003, ApJ, 593, 235  
 Wolfe A. M., Gawiser E., Prochaska J. X., 2005, ARA&A, 43, 861  
 Wolfe A. M., Howk J. C., Gawiser E., Prochaska J. X., Lopez S., 2004, ApJ, 615, 625  
 Wolfire M. G., Hollenbach D., McKee C. F., Tielens A. G. G. M., Bakes E. L. O., 1995, ApJ, 443, 152